2008 IEEE International Conference on
Robotics and Automation
Pasadena, CA, USA, May 19-23, 2008

Towards Spatial and Semantic Mapping in Aquatic Environments

Victor L. Chen, Maxim A. Batalin, William J. Kaiser, Gaurav Sukhatme
Electrical Engineering Department
University of California, Los Angeles
Email: victorc@ucla.edu

Abstract— **High fidelity data acquisition of dynamic spatiotemporal phenomena for aquatic environmental research suggests the use of actuated sensors. Furthermore, characterization of the floor in aquatic environments is beneficial for environmental science, as well as can be applied to robot localization. The NIMS AQ cable robot platform is designed to meet these requirements and satisfy the constraints of large scale, in-field deployments. In addition to a set of water quality sensors it also carries an ultra-miniature side-scan sonar. In this paper we show the development of methods for autonomous range detection, spatial and semantic mapping in underwater environments. These methods are demonstrated to be important for future developments including localization, navigation, and path planning, particularly for 3D mobility. Experiments have been performed in both controlled environments and a lake environment and results are discussed.**

I. INTRODUCTION

There is a critical need in aquatic environmental research for acquisition of high fidelity data of the spatiotemporally varying phenomena. A fundamental requirement of being able to adapt to changes in the environment suggests the use of actuated sensors - robots carrying environmental sensors. In aquatic environments, the floor (riverbed, bottom of the ocean, etc.) plays a very important role as it can be used by the mobile robot for localization. Moreover, understanding the topology and sediment characteristics in the aquatic floor allows environmental scientists to answer many questions pertaining to the hydrology and geomorphology.

In the past we have proposed Rapidly Deployable NIMS (NIMS RD) cable based robotic systems that were used for a number of terrestrial [1] as well as aquatic applications, pertaining to the study of biological phenomena and contaminant distributions in aquatic environments [2], [3], [4]. Experience gained in these campaigns led to the development of an aquatic NIMS system, referred to as NIMS AQ [5]. NIMS AQ presents a solution to many of the limitations of operating older iterations of NIMS systems in aquatic environments. The NIMS AQ sensor suite includes a set of water quality probes as well as an acoustic submersible sonar [6]. The sonar has multiple tunable parameters as well as a 360° field of view.

Processing of sonar reflection data is not limited to range detection. The intensity of the reflection can be used to determine the reflection coefficient as a ratio of the intensities of the incident and reflected waves on the sediment surface. This information can be used to determine an estimate of the distribution of the sediment composition. Although more complex [7] and precise methods have been developed for acoustic inversion of subsurface sediments, they require specialized sonar instruments capable of high bandwidth, low frequency pulse transmissions. Since these sonar instruments are typically quite large in size, these methods are not feasible given the physical constraints of our system and application domain.

Spatial and semantic characterization (mapping) are important from a systems perspective as in the future they will be critical for localization of the NIMS AQ platform as well as for navigation and path planning, particularly for 3D mobility. Additionally, from a science perspective, spatial and semantic maps collected over time can give insight into the hydrology and geomorphology of aquatic environments.

There has been considerable interest in spatial mapping of both aquatic environments [8], [9] and terrestrial environments [10], [11], [12]. Similarly, subsurface sediment characterization has been a focus of the marine acoustics and geophysics fields [7], [13], [14]. To the best of our knowledge, this is the first work reporting results on successful semantic characterization of the aquatic environment floor using an autonomous vehicle and a miniature sonar. This paper also describes our initial work in the application of the mobility provided by NIMS AQ combined with capabilities of the sonar for depth profiling, aquatic floor 3D spatial and semantic characterization (mapping).

II. EXPERIMENTAL PLATFORM: NIMS AQ CABLE-DRIVEN ROBOT

The Aquatic Networked InfoMechanical Systems platform (NIMS AQ) [5] is the latest in the family of NIMS systems [1], [15], [16], developed specifically for increasing demands in aquatic applications. These include sampling larger cross-sections of the aquatic environments and providing increased spatial coverage through multiple cross-sections spread over a large spatial domain. NIMS AQ improves upon the previous NIMS designs by providing reduced setup time, lower tension requirements on the supporting cableway, reduced dependency on the specific support infrastructure, and reduced physical footprint. These characteristics make it an ideal platform for several important aquatic sensing applications.

Figure 1(a) displays a schematic representation of NIMS AQ. The system is comprised of a rigid sensing tower supported by two Hobie FloatCat pontoons (developed by Hobie Cat Company) in a catamaran configuration. An

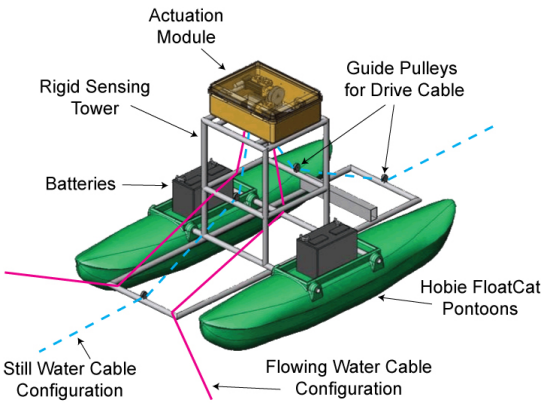

(a) Schematic Representation

(b) Image captured in the field

Fig. 1. Aquatic Networked InfoMechanical System (NIMS AQ).

Fig. 2. Ultra-miniature scanning sonar developed by Imagenex Corp.

actuation module resides on top of the sensing tower that drives the horizontal cable and vertical payload cable for the horizontal and vertical motion, respectively, across a cross-section of the aquatic environment. The vertical cable enables actuation of the sensing payload, along the vertical column of water, from the water surface to the floor of the aquatic environment. Power for the system is provided by two deep cycle marine batteries housed on top of the pontoons. The horizontal drive cable is kept center-aligned to the craft by using guide pulleys that can be repositioned based on the aquatic environment in which NIMS AQ is sampling (flowing or still water conditions).

The current version of NIMS AQ was designed as a prototype system to test the fundamental system requirements including actuation, sensor interfaces, and network communications. NIMS AQ currently is capable of determining its own position as well as execute autonomous algorithms and actuate the horizontal and vertical cables, effectively providing a 2D transect for positioning the sensor. The next version of NIMS AQ will inherit several of these system components and features with an additional capability to provide three-dimensional mobility. It will use multiple cables, similar to the three-dimensional NIMS platform [16], to provide the ability to sample the surface of aquatic environments, along with vertical actuation of the sensor payload. Such capabilities demand a further reduction in setup times and accurate localization.

The current prototype version of NIMS AQ is equipped with a suite of water quality sensors as well as with a submersible sonar [6]. Figure 2 displays the sonar that is used with the current system. It is a commercial miniature side-scan sonar unit developed by Imagenex Corp and operates in either one of the two frequencies - 675 kHz and 850 kHz. The sensor head and electronics are housed in a cylindrical body 2 inches in diameter and 3 inches in height. The small physical profile helps minimize the physical footprint of the sensor payload and that of the NIMS AQ system as a whole, in order to perform sampling with minimal disturbance to the biological or chemical phenomena.

III. Sonar Signal Processing and Aquatic Floor Characterization

In this section we describe the fundamentals in range estimation and sonar data processing techniques. We also describe our initial implementation of algorithms that use sonar processed data for spatial and semantic characterization (mapping).

A. Range Estimation

An ideal output signal from the sonar would consist of a delta function corresponding to the two-way travel time between the sonar and the reflection surface. However, output signals from the sonar can vary considerably with different environments and even within the same environment if the subsurface structure and composition is heterogeneous. This requires robust processing of the signals in order to reliably extract accurate range information in the presence of noise, weak reflections, multipath reflections and other non-ideal conditions. To cope with variation in signal output, a procedure involving a series of computational filters is employed to reduce the probability of an incorrect range estimation. These filters will be referred to as the nearest neighbor (NN), multipath reflections (MR), and expected range (ER) filters. The procedure is illustrated on an example output signal in

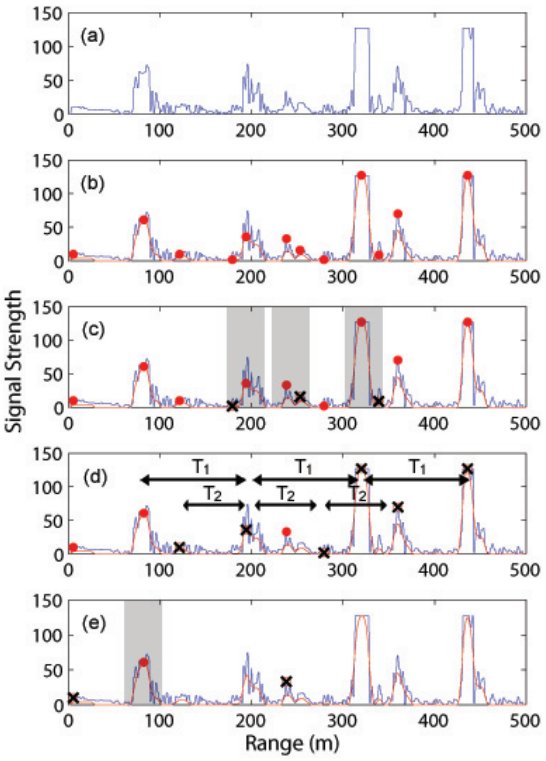

Fig. 3. Procedure for estimation of range from example reflection signal after application of each filter. From top to bottom: the raw signal; raw signal with smoothing spline and maxima identified; raw signal with smoothing spline and maxima after NN filter applied; raw signal with smoothing spline and maxima after NN and MR filters applied; raw signal with smoothing spline after NN, MR and ER filters applied.

Figure 3 and its effectiveness will be discussed with results in Section 4.

Figure 3(a) shows an example of a raw sonar output signal. In the first step of the procedure, a cubic spline interpolant [17] is applied to the time-series output signal which uses a smoothing coefficient selected pre-runtime that effectively filters high frequency noise while preserving the structure of the signal. This allows for straightforward identification of local maxima. Figure 3(b) shows the spline function and the maxima values identified. The resulting set of maxima values contains a range value which will have a high probability of corresponding to the first reflection of the transmitted pulse off of the reflecting surface of interest.

In aquatic environments, suspended sediments can form gradients above the actual floor. These sediment gradients can cause scattering of the acoustic pulse and interference that will result in the output signal containing highly colocated maxima, even after applying the smoothing spline. In the open ocean, these gradients are negligible relative to the depth. However, these errors are particularly pronounced in lake environments which are relatively shallow and do not experience significant mixture effects. In other cases, a weak reflection may be viewed as noise and liable to be neglected by the smoothing spline. Thus, the smoothing coefficient must be chosen to balance the expected noise levels with the expected return strength. Future work will examine water turbidity to determine any correlation with sonar signal noise.

After a set of maxima has been identified, there may be several maxima values which are highly colocated but only one of which corresponds to the actual reflection off the floor. To resolve this, the NN filter is applied. By assuming a minimum distance between the floor and water surface, a sliding window can be set where the strongest maxima will be selected over neighboring maxima falling within this window. This is shown in Figure 3(c). In our current procedure, the window size is static, however a dynamic window size that varies based on the expected depth and environmental characteristics may yield more accurate results. We plan to also investigate this in our future work.

Often, the first maxima in the time series will correspond to the reflecting surface and will have the highest intensity, however this is not always the case. Depending on the characteristics of the fluid environment, reverberation can occur resulting in unusually high reflections occurring in the space immediately surrounding the sonar. In some environments characterized by surfaces with high reflection coefficients, the pulse emitted from the sonar will resonate between the floor and the water surface producing multipath reflections increasing in intensity. In order to identify the periodicities corresponding to resonant frequencies of the signal-space we apply the MR filter. This is done by computing the periodogram of the output signal using the Fast Fourier Transform (FFT) [18]. Knowing these periodicities, we can identify and eliminate maxima corresponding to multipath reflections, regardless of their relative intensities as shown in Figure 3(d).

Assuming depth profile information and accurate localization are available, we can apply the ER filter. The ER filter operates by setting a window corresponding to the expected range such that maxima falling outside this window are eliminated as shown in Figure 3(e). Although this filter relies on localization information which may not always be accurate, it can produce the greatest percent reduction in the size of the point cloud, as discussed in the results.

B. Spatial Characterization (Mapping)

NIMS AQ allows actuation to be exploited for spatial characterization of the subsurface environment. In some sense, spatial characterization is merely an extension of the system's ability to detect range. For the purposes of spatial characterization, mobility of the NIMS AQ platform is constrained to a 1D line. However, the sonar is able to acquire range information r at a specified angle θ, which, along with the NIMS AQ position $(x_p,\ z_p)$, completes the cylindrical coordinate system. We can transform these cylindrical coordinates to cartesian coordinates, taking into account that in our design the cylindrical coordinate system

Algorithm:updateMap

Input: $Threshold$, $minValue$, i, locations: $l_1, \ldots, l_i$, k cells: $c_1, \ldots, c_k$, Cell Probability: $P(c_1), \ldots, P(c_k)$, Location Intensity: $I(l_1), \ldots, I(l_i)$
Output: Updated probabilities: $P(c_1), \ldots, P(c_k)$
begin
  foreach *maxima* m_i **do**
    foreach *maxima* m_j *such that* $m_j \neq m_i$ **do**
      if $|m_j - m_i| > nn_window$ **then**
        if c_m *contains* l_j *and* c_m *exists* **then**
          Increment P(c_m);
        else
          add c_m to cell list;
      else
  return $P(c_1), \ldots, P(c_k)$;
end

Algorithm 1: updateMap: Algorithm for updating the cell probabilities in the map.

is effectively rotated 90° on its side, using the equations

$$\begin{aligned} x &= x_p \\ y &= r\cos(\theta) \\ z &= r\sin(\theta) + z_p \end{aligned} \tag{1}$$

As the sensor scans the environment and the reflection signals are processed, these points are added to or removed from a dynamically allocated hashtable using an occupancy grid algorithm [19], [10]. The (x, y, z) triplet is used as a key for its associated probability value, i.e. the probability that the coordinate is occupied in the spatial map. An infinite number of key values is possible yet it is not feasible nor effective to store each unique key that arises. To satisfy this, the space is discretized into a finite number of uniformly sized cells. For each point falling within the space bounded by the cell, the probability of the cell being occupied increases. If the probabilty of the cell decreases past a certain threshold, the key corresponding to the cell is removed from the hash table to ensure that hash table contains only information about the occupancy of the map and not about the vacancy. Hence, the information about the 3D map of the aquatic floor is saved efficiently in memory. The cell update algorithm is described in Algorithm 1.

C. Sediment Physical Properties Estimation and Semantic Characterization (Mapping)

Traditional approaches for estimating the physical properties of subsurface sediment typically require sonar devices which operate at low frequencies and with wide bandwidth, e.g. in the range between 100 Hz and 10 kHz [7], [14]. At these frequencies, the pulses emitted from the sonar are able to penetrate the uppermost sediment layer to sediment layers located tens of meters below. This allows for the calculation of the attenuation rolloff of the sediment layer which is calculated as the least squares slope of the attenuation as a function of frequency. The attenuation rolloff is highly correlated to the permeability of the sediment layer, which is obtained from a plot of attenuation rolloff against permeability, generated using an estimated porosity measurement [7].

Another important value in the inversion procedure is the reflection coefficient [7] of the sediment and is calculated using

$$R = 10\log\left(\frac{\langle I_{seabed/water}\rangle {r^2}_{seabed/water}}{\langle I_{air/water}\rangle {r^2}_{air/water}}\right) \tag{2}$$

The reflection coefficient is highly correlated to the porosity of the sediment layer. An estimate of porosity is obtained from a reflection coefficient-porosity plot generated from the expected permeability. This estimate is then used to generate a new attenuation rolloff-permeability plot in order to refine the permeability estimate. The porosity and permeability calculations are reiterated until they converge on a solution. They are then used to calculate the mean grain size and other acoustic properties of the sediment [7].

Sonars used for sediment classification are typically large instruments designed to be towed on ships for deep water oceanographic studies [20], [21] as compared to the sonar device used on the NIMS AQ platform. While its small profile makes it ideal for use on lake and river environments and on the NIMS AQ platform, it is capable of operating only at 675 kHz and 850 kHz. At these frequencies, it is not feasible to determine the attenuation rolloff. In addition, at this high frequency, pulses emitted from the sonar will not penetrate the top sediment layer making it unfeasible to determine the attenuation. We can, however, apply the formula for determining the reflection coefficient which will provide an estimate of the composition of the subsurface sediment, as described in the next section.

IV. Deployments and Results

Several experiments were performed using the sonar in controlled environments (swimming pool and in a large water tank). In addition, experiments were performed using the sonar attached to the NIMS AQ platform at an artificial lake on the UC Merced campus to test the accuracy of the sonar for depth profiling and spatial mapping and to test the feasibility of using the sonar for semantic mapping in a real environment.

A. Depth Profiling

In the first experiment, conducted at the UC Merced lake, the sonar was mounted at a fixed depth 6 cm below the NIMS AQ platform and sampling was performed at 2 meter intervals along a 70 meter transect. Simultaneously, a sensor payload consisting of a Hydrolab [22] water quality multisensor, which is equipped with a depth sensor, was lowered vertically from the platform until tension in the lowering cable was observed to decrease significantly, indicating contact with the lake bed. Similarly, a third measurement was produced by lowering a weight attached to a flexible measuring tape until the tension in the measuring tape was observed to reach a low threshold. In the case of the hydrolab, position was controlled by the NIMS AQ platform whereas in the case of the measuring tape, position was controlled by an operator in a kayak. Although these methods use cable slack as a proxy for indicating contact of the payload with the sediment

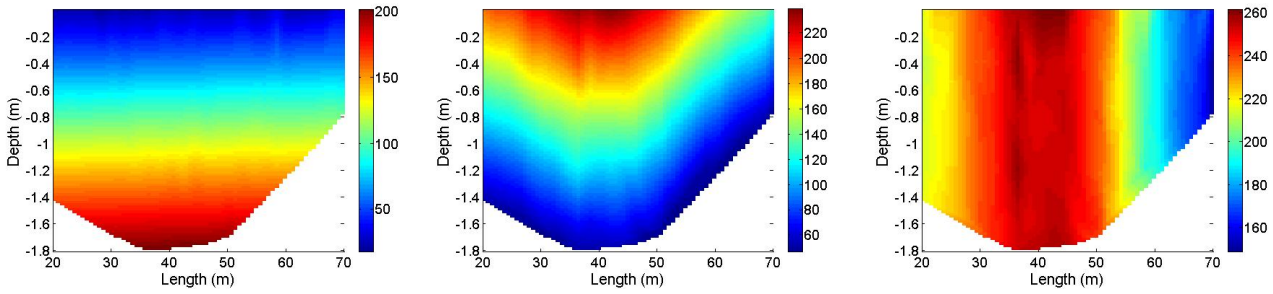

Fig. 5. Colormaps of subset of range estimates from sonar to water surface, range estimates from sonar to lake bottom, and full depth of water column, respectively, on part of the executed transect. The full depth is computed by addition of the range estimate from the sonar to the water surface and the range estimate from the sonar to the lake bottom.

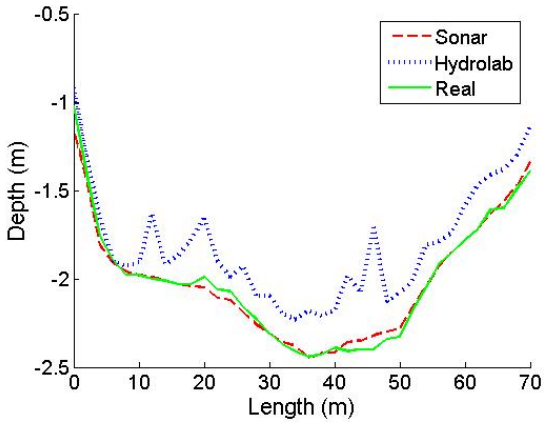

Fig. 4. Comparison of depth measurements from sonar, hydrolab, and tape measure.

surface, they provide reasonable estimates of the depth at each position. Particularly for the tape measure method, the operator can make use of tension control via his hands and intuition as opposed to computer controlled motors lacking tension feedback which cannot.

The results demonstrate that the sonar is accurate to within ± 10 cm of the ground truth measurements provided by the tape measure, as shown in Figure 4. In addtion, although the Hydrolab depth measurements are inaccurate, they are consistent with the measurements taken from the sonar and the tape measure.

In the next experiment, the sonar was attached to the sensor payload and sampled with the sonar head trained upward at the water surface and downward at the lake floor, for each raster point. The purpose of this experiment was to verify that range estimates from the sonar are consistent for different depths. Figures 5(a) and 5(b) show the range estimates from the sonar to the lake bed and the range estimates from the sonar to the water surface, respectively. Figure 5(c) shows the full depth of the water column calculated at each raster point by adding the range measurements to the water surface and to the lake floor. The distribution of depth values is clearly consistent with the depth profile resulting in a horizontal stratification of the depth values. From this data we can infer that the calculation of depth using the sonar does not vary with depth and can reliably report range information regardless of where the sonar is located within the transect. This information can further be used to more accurately localize the position of the sensor payload within the transect.

B. Spatial Mapping

In many natural and large body aquatic environments, it is often difficult to observe the floor visually due to the absorption of light and quality of water. In order to verify the accuracy of the sonar, an experiment was performed in a swimming pool located on the UCLA campus. The swimming pool provided an environment which allowed us to control the placement of several objects within the pool and collect photographic evidence in order to compare the results. A large water bottle and several rugged equipment cases varying in size and shape were distributed throughout a section of the pool. Using the sonar, a scan was performed over the area and the surface reconstruction was calculated in post processing. Objects appearing in the surface reconstruction accurately correspond to objects in the environment in size, position and orientation. The experimental setup and results are illustrated in Figure 7.

The results of the spatial mapping experiment in the swimming pool enabled us to proceed with operation in a natural environment. In order to reconstruct 3D maps of the lake bottom, the sonar was mounted on the NIMS AQ platform at a fixed depth below the water surface and oriented such that the scanning plane of the sonar was normal to the transect plane and to the water surface. The sonar collected reflection data at 3° intervals over a 90° arc centered at normal incidence to the lake bottom, and repeated this sampling at 2 meter intervals along the 70 meter transect.

Figure 6 shows an example surface reconstruction of the lake bed on part of the executed transect. By comparing the depth of the surface as a function of the length with the data from the depth profiles collected by the sonar and the tape measure in Figure 4, it is sufficient to conclude that the reconstruction is accurate. In addition, since the transect was chosen near the center of the lake, we would not expect to observe much of a 'bowl' effect but rather that

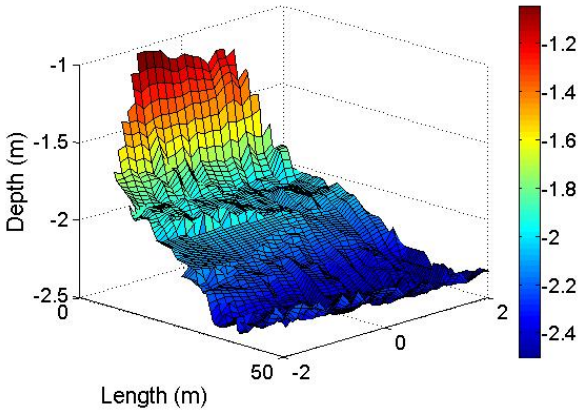

Fig. 6. Example of the spatial map acquired using the NIMS-AQ platform on a part of the executed transect. The depth reported by the sonar as indicated by the surface color is consistent with the position of the z-axis.

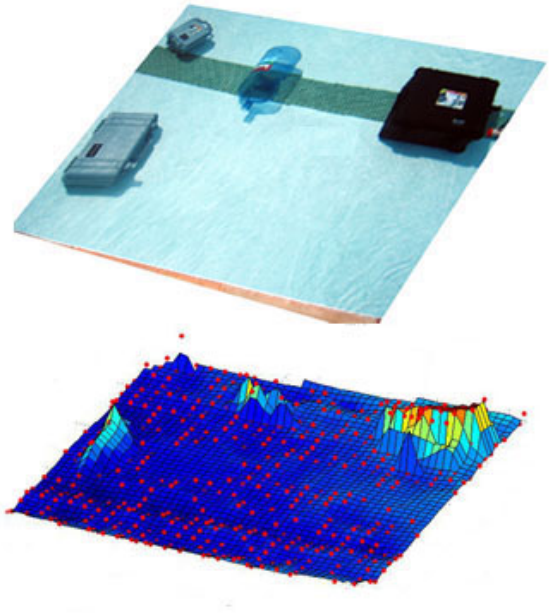

Fig. 7. Example of the sonar's ability to resolve more dynamic environments.

the lateral variation be relatively small (i.e. flat along the y-axis) as shown. However, a slight down-sloping gradient is observable in the positive direction on the y-axis in the surface reconstruction, consistent with the position of the transect.

The performance of each computational filter can be measured by the percent reduction in the number of points in the point cloud resulting from the application of each filter. The size of the point cloud and percent reduction in the number of points resulting from each of these filters is summarized in Table I. The point clouds resulting from each filter are illustrated in Figures 8(a) to 8(f).

In this example, the contribution of the MR filter to the number of points reduced is miniscule. However, in a natural

TABLE I

NUMBER OF POINTS IN THE POINT CLOUD AND PERCENT REDUCTION IN SIZE AFTER APPLICATION OF NEAREST NEIGHBORS (NN), MULTIPATH REFLECTIONS (MR), EXPECTED RANGE (ER) FILTERS.

Filters Applied	Number of Points	Percent Reduction
∅	2741	0.00%
NN	2049	25.25%
MR	2058	24.92%
ER	1925	29.77%
NN, MR	2032	25.87%
NN, ER	1710	37.61%
NN, MR, ER	1705	37.80%

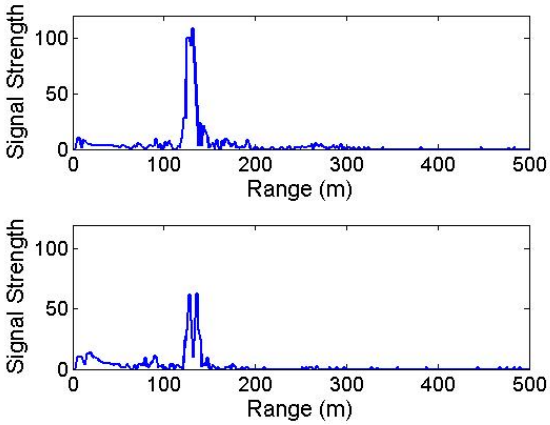

Fig. 9. Examples of output signals of sonar aimed at sand (above) and clay (below) acquired using the same experimental setup.

environment such as a lake, this is to be expected as most of the pulse energy will be absorbed by the lake floor to prevent resonance.

C. Semantic Mapping

Before proceeding to operate in a real environment, an experiment was performed using a large water tank (capable of holding 180 gallons) as a controlled environment. This setup allowed us to test the feasibility of using the sonar for semantic characterization using sediments with known qualities. The tank was filled with water and several inches of two sediments: sand and a sand/clay mixture. The sonar was used to acquire reflection signals from the two sediments, examples of which are shown in Figure 9. In this example, the intensity of the reflection from sand, and consequently the reflection coefficient, is clearly higher than the intensity of the reflection from the clay. This is consistent with observations from the literature [23].

The results of water tank experiment demonstrated that it was feasible to use the sonar for semantic characterization of aquatic environments. To test this in the lake environment, the sonar was attached to the sensor payload using NIMS AQ and sampled with the head trained upward at the water surface and downward at the lake bed. The reflection is calculated as a ratio of the intensities of the reflected and incident sonar pulses (using water surface reflection intensity

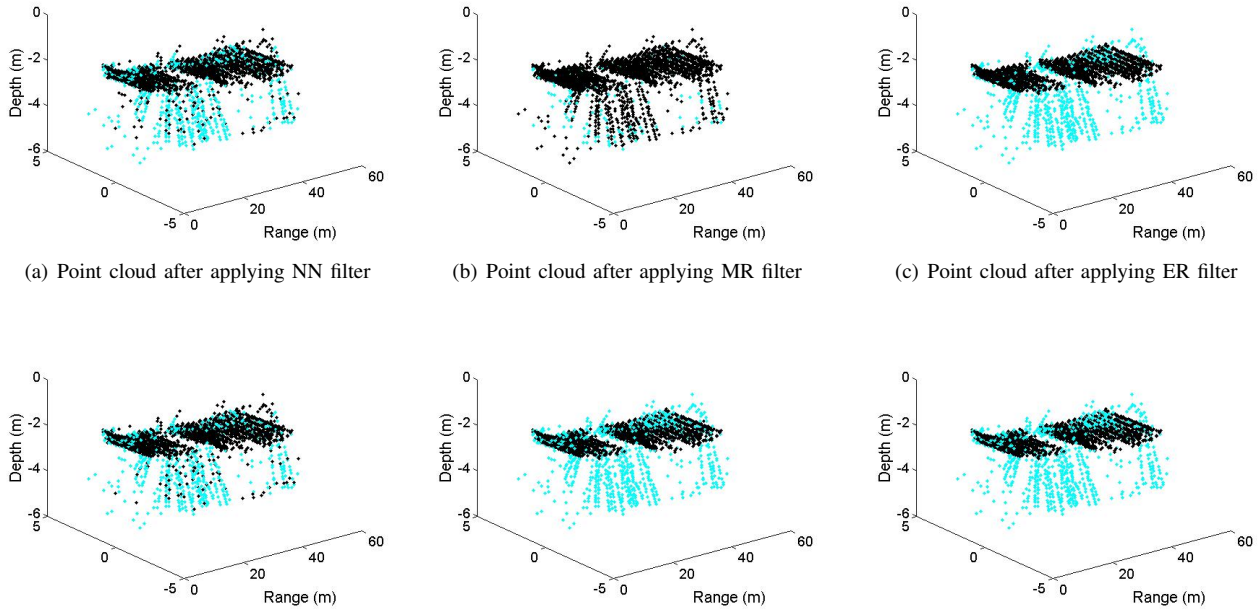

(a) Point cloud after applying NN filter

(b) Point cloud after applying MR filter

(c) Point cloud after applying ER filter

(d) Point cloud after applying NN and MR filters

(e) Point cloud after applying NN and ER filters

(f) Point cloud after applying NN, MR, and ER filters

Fig. 8. Resulting points clouds (shown in black) after applying NN, MR, and ER filters to the unfiltered point cloud (shown in blue).

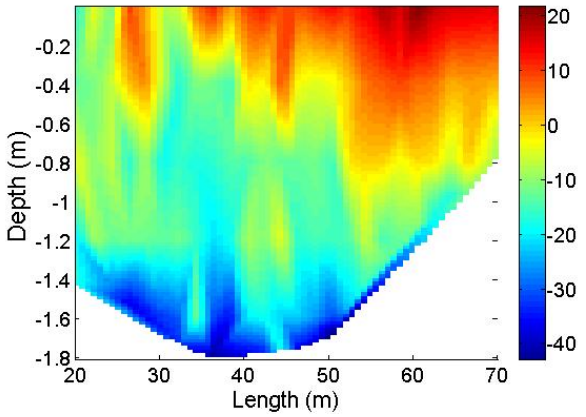

Fig. 10. Reflection coefficient distribution along the lake transect.

as a substitute for incident pulse intensity), using Equation 2, and depends on the range of the sonar to the lake bed and to the water surface. Figure 10 shows the reflection coefficient of the sediment calculated at each raster point in the transect. While the reflection coefficient varies with depth, this variation is inconsistent and the distribution of the reflection coefficient along a constant depth is also not consistent with the distribution of the depth measurements. This suggests that the reflection coefficient is not solely a function of depth and could represent some physical or acoustic property of the lake sediment.

Further inspection reveals that there is a general trend on the reflection coefficient. At any given depth, with the depth held constant, the reflection coefficient tends toward lower values near the deepest sections of the lake, gradually increasing towards the near end and increasing sharply at the far end at approximately 50 meters. This suggests that the sediment occupying the deeper regions of the transect is absorbing more of the pulse energy whereas the shallower regions are reflecting more of the pulse energy.

TABLE II

QUALITATIVE SUMMARY OF THE COMPOSITION OF SOIL SAMPLES ACQUIRED FROM EXECUTED TRANSECT.

Distance	Description
50 m	mud
55 m	mud
65 m	mud with dense rocks
68 m	mud with dense rocks

Samples of the lake sediment were collected at several points along the transect using a soil core sampler [24]. Due to the difficulty of operating the core sampler at the depth of the lake, only samples closer to the banks were extracted. Additionally, the samples were collected following the experiment so the distances at which the samples were collected are appoximately the same relative to the executed transect. Table II summarizes qualitatively the composition of the sediment samples. From this information we can extrapolate that the concentration of rocks decreases towards the center of the transect and is consistent with the reflection coefficient distribution in Figure 10 calculated from the sonar output.

V. Conclusion and Future Developments

In this paper we described an application for underwater ultrasonic sonar used on the NIMS AQ robotic platform. We presented methods for robust range estimation from noisy and inconsistent sonar reflection data and initial results in spatial and semantic mapping. We tested these methods in controlled environments as well as in a real lake.

The experimental trials performed so far have shown successful results in range detection, spatial, and semantic (sediment) mapping. However, more rigorous experimental trials are currently underway. While the semantic mapping information will be used by the environmental scientists to inform their models, the spatial mapping will be used for localization and navigation of the next generations of NIMS AQ. Our objective for NIMS AQ is development of a fully autonomous aquatic sensing robot. This requires integration with the sonar in order to achieve accurate localization and reliable navigation. Features such as dynamic sonar parameter selection may be added to ensure high contrast output signals in order to enable more robust signal processing.

Acknowledgment

This material is based upon work supported in part by the US National Science Foundation (NSF) under Grants ANI-00331481. Any opinions, findings, and conclusions or recommendations expressed in this material are those of the authors and do not necessarily reflect the views of the NSF. The authors would like to acknowledge and thank Amarjeet Singh for his comments to improve the content of this paper, as well as Henry Pai and Chris Butler for their support in investigative field work.

References

[1] B. L. Jordan, M. A. Batalin, and W. J. Kaiser, "Nims rd: A rapidly deployable cable based robot," in *IEEE International Conference on Robotics and Automation (ICRA)*, Rome, Italy, April 2007.

[2] A. Singh, M. A. Batalin, V. Chen, M. J. Stealey, B. Jordan, J. Fisher, T. Harmon, M. Hansen, and W. J. Kaiser, "Autonomous robotic sensing experiments at san joaquin river," in *IEEE International Conference on Robotics and Automation (ICRA)*, Rome, Italy, April 2007.

[3] A. Singh, M. A. Batalin, M. J. Stealey, B. Zhang, A. Dhariwal, B. Stauffer, S. Moorthi, C. Oberg, A. Pereira, V. Chen, Y. Lam, D. Caron, M. Hansen, W. J. Kaiser, and G. Sukhatme, "Human assisted robotic team campaigns for aquatic monitoring," *Journal of Field Robotics, Special Issue on Teamwork in Field Robotics*, pp. accepted, to appear, 2007.

[4] T. C. Harmon, R. F. Ambrose, R. M. Gilbert, J. C. Fisher, M. Stealey, and W. J. Kaiser, "High-resolution river hydraulic and water quality characterization using rapidly deployable networked infomechanical systems (nims rd)," *Environmental Engineering Science*, vol. 24, no. 2, pp. 151–159, 2007.

[5] M. J. Stealey, M. A. Batalin, and W. J. Kaiser, "Nims-aq: A novel system for autonomous sensing of aquatic environments," in *IEEE International Conference on Robotics and Automation (ICRA)*, 2008, p. submitted.

[6] "Imagenex model 852 ultra-miniature scanning sonar," 2007. [Online]. Available: http://www.imagenex.com/Downloads/What_s_New/852_Ultra-Miniature/852_ultra-miniature.html

[7] S. G. Schock, "Remote estimates of physical and acoustic sediment properties in the south china sea using chirp sonar data and the biot model," *IEEE Journal of Oceanic Engineering*, vol. 29, no. 4, 2004.

[8] C. J. Browna, K. M. Coopera, W. J. Meadowsb, D. S. Limpennya, and H. L. Reesa, "Small-scale mapping of sea-bed assemblages in the eastern english channel using sidescan sonar and remote sampling techniques," *Estuarine, Coastal and Shelf Science*, vol. 54, pp. 263–278, 2002.

[9] D. J. Keith, V. Capone, G. S. Cook, D. A. Carey, D. N. Wiley, and J. P. Fish, "Target detection and mapping of aquatic hazardous waste sites in massachusetts bay utilizing sidescan sonar," in *OCEANS Mastering the Oceans Through Technology*, vol. 1, 1992, pp. 497–502.

[10] H. P. Moravec and A. Elfes, "High resolution maps from wide angle sonar," in *IEEE International Conference on Robotics and Automation*, 1985, pp. 116–121.

[11] P. M. N. J. J. Leonard and R. J. Rikoski, "Towards constant-time slam on an autonomous underwater vehicle using synthetic aperture sonar," in *Springer Tracts in Advanced Robotics*, 2005, pp. 409–420.

[12] S. Williams and I. Mahon, "Simultaneous localisation and mapping on the great barrier reef," in *IEEE International Conference on Robotics and Automation*, 2004, pp. 1771–1776.

[13] E. L. Hamilton, "Reflection coefficients and bottom losses at normal incidence computed from pacific sediment properties," *Geophysics*, vol. 35, no. 6, 1970.

[14] A. Turgut, M. McCord, J. Newcomb, and R. Fisher, "Chirp sonar sediment characterization at the northern gulf of mexico littoral acoustic demonstration center experimental site," *Oceans '02 MTS/IEEE*, vol. 4, 2002.

[15] R. Pon, M. Batalin, J. Gordon, M. Rahimi, W. Kaiser, G. Sukhatme, M. Srivastava, and D. Estrin, "Networked infomechanical systems: A mobile wireless sensor network platform," in *IPSN*, 2005, pp. 376–381.

[16] P. H. Borgstrom, M. J. Stealey, M. A. Batalin, and W. J. Kaiser, "Nims3d: A novel rapidly deployable robot for 3-dimensional applications," in *IEEE/RSJ International Conference on Intelligent Robots and Systems*, Beijing, China, 2006.

[17] C. H. Reinsch, "Smooth by spline functions," *Numerische Mathematik*, vol. 10, no. 3, 1967.

[18] A. Schuster, "On the invesigation of hidden periodicities," in *Terr. Mag. Atmos. Elect.*, 1898, pp. 13–41.

[19] A. Elfes, "Using occupancy grids for mobile robot perception and navigation," *Computer*, vol. 2, no. 6, pp. 46–57, 1989.

[20] D. A. Mindell and B. Bingham, "A high-frequency, narrow-beam sub bottom profiler for archaeological applications," *Proceedings of IEEE Oceans 2001 Conference*, 2001.

[21] J. A. Grant and R. Schreiber, "Modern swathe sounding and sub-bottom profiling technology for research applications: The atlas hydrosweep and parasound systems," *Marine Geophysical Researches*, vol. 12, no. 1,2, 1989.

[22] "Hydrolab minisonde 5," 2007. [Online]. Available: http://www.hydrolab.com/products/hydrolabms5.asp

[23] L. R. LeBlanc, L. Mayer, M. Rufino, S. G. Schock, and J. King, "Marine sediment classification using the chirp sonar," *The Journal of the Acoustical Society of America*, vol. 91, no. 1, pp. 107–115, January 1992.

[24] "Soil core sampler," 2007. [Online]. Available: http://www.soilmoisture.com/prod_details.asp?prod_id=76&search=1